Fizika Nizkikh Temperatur, 2009, v. 35, No. 7, p. 725–734

Nanoparticles effect on magnetic and transport properties of $(La_{0.7}Sr_{0.3})_{0.9}Mn_{1.1}O_3$ manganites

V. Dyakonov[1,2], A. Ślawska-Waniewska[1], J. Kazmierczak[1], E. Zubov[2], S. Myronova[2], V. Pashchenko[2], A. Pashchenko[2], A. Shemjakov[2], V. Varyukhin[2], S. Prilipko[2], V. Mikhaylov[2], K. Piotrowski[1], Z. Kravchenko[2], O. Iesenchuk[1], A. Szytuła[3], W. Bazela[4], and H. Szymczak[1]

[1]*Institute of Physics PAS, 32/46 Al. Lotników, 02-668 Warsaw, Poland*

[2]*A.A. Galkin Donetsk Physico-Technical Institute NANU, 72 R. Luxembourg Str., Donetsk 83114, Ukraine*
E-mail: dyakon@ifpan.edu.pl

[3]*M. Smoluchowski Institute of Physics, Jagiellonian University, Reymonta 4, 30-059 Kraków, Poland*

[4]*Institute of Physics, Technical University, Podchorążych 1, 30-084 Kraków, Poland*

Received March 24, 2009

We report on the magnetic and transport thermal measurements of nanosize $(La_{0.7}Sr_{0.3})_{0.9}Mn_{1.1}O_3$ manganite. The nanoparticles were synthesized with use of co-precipitation method at different (800, 900 and 950 °C) temperatures. Their crystal structure was determined to be perovskite-like with a rhombohedral distortion (the space group $R\bar{3}c$). The phase composition and specific surface nanopowders were determined. The average size of synthesized nanoparticles (from 40 to 100 nm) was estimated by both the method of low-temperature adsorption of argon and x-ray diffraction measurements. All the nanosize samples show ferromagnetic-like ordering with close phase transition temperatures. Their magnetization decreases with reducing the particle size. Comparison of experimental and calculated temperature dependences of the spontaneous magnetic moment shows that the spontaneous magnetization both in magnetic field and without field is well described in the frame of the double exchange model. The decrease of magnetization with decreasing particle size is due to increasing the surface contribution to magnetization. The magnetic entropy was shown to increase with increasing applied magnetic field and to be smaller for the small particles. The resistivity was established to become higher with reducing the particles size at any temperatures.

PACS: *65.05.cp* X-ray diffraction;
61.46.–w Structure of nanoscale materials;
61.50.Ks Crystallographic aspects of phase transformations; pressure effects;
62.50.–p High-pressure effects in solids and liquids;
75.47.Gk Colossal magnetoresistance;
75.75.+a Magnetic properties of nanostructures.

Keywords: nanostructures, manganite, magnetic measurement, resistance.

Introduction

At present, the most interesting metal-oxide materials are rare-earth manganites with the chemical composition of $(RE_{1-x}M_x)_yMn_{1+y}O_3$, where RE = La, Pr, Nd, and M = = Sr, Ca, Ba, manifesting the colossal magnetoresistive (CMR) effect [1–3]. Their studies were performed mainly on bulk materials (ceramic, single crystals) and thin films. Physical properties of mixed valent perovskite manganites were shown to depend crucially on both doping level and the nature of doping element as well as on various intrinsic inhomogeneities among which the nanostructure deserves the special attention. Due to small size, these nanocrystallites exhibit novel properties which are significantly different from those of the bulk material. One important factor is increasing surface to volume of the grains ratio as the particle sizes reduce to the nanoscale. As a result, the small-size effect

© V. Dyakonov, A. Ślawska-Waniewska, J. Kazmierczak, E. Zubov, S. Myronova, V. Pashchenko, A. Pashchenko, A. Shemjakov, V. Varyukhin, S. Prilipko, V. Mikhaylov, K. Piotrowski, Z. Kravchenko, O. Iesenchuk, A. Szytuła, W. Bazela, and H. Szymczak, 2009

and surface effect perturb the structure and properties of nanoparticles. The intensive discussions devoted to synthesis, characterization of nanosized manganites, study the influence of nanodimension grains on the magnetism and transport of manganites as well as their application are present in the Refs. 4–16. dc magnetization measurements of nanosize (the average particles size of 35 nm) $La_{0.3}Ca_{0.7}MnO_3$ manganite did not show significant change of the magnetic phase transition temperature in respect to its bulk counterpart [4]. The magnetization measurements of $La_{5/8-0.3}Pr_{0.3}Ca_{3/8}MnO_3$ (LPCMO) manganite under pressure up to 9.5 kbar have shown that pressure effect on ferromagnetic ordering in nanopowder (the grain sizes from 40 to 1000 nm) LPCMO is similar to that obtained for bulk samples [5]. An applied pressure enhances the phase transition temperature of $La_{1-x}MnO_{3+d}$ particles (20–30 nm) with a pressure coefficient of $dT_C/dP \approx 1.4$–1.9 kbar^{-1} [6]. The 30 nm nanoparticles of $La_{0.7}Sr_{0.3}MnO_3$ (LSMO) also exhibit the Curie temperature close to stoichiometric phase-pure LSMO [7]. A reduction of grain size in the $La_{0.7}Sr_{0.3}MnO_3$ [8] and $La_{2/3}Ca_{1/3}MnO_3$ [9] compounds was found to decrease magnetization due to increasing ratio of surface to volume of the grains. The grain size (from 53 to 8 nm) induced variations in structural and magnetic properties observed in $La_{0.8}Sr_{0.2}MnO_3$ nano-ferromagnet indicate a very important role of the particle surface effects [10]. The temperature dependences of magnetization of $La_{0.8}Sr_{0.2}MnO_3$ show that the nanoparticles with the grain size below 25 nm exhibit superparamagnetic behavior. Magnetic resonance spectra have been studied to obtain microscopic information on the magnetic structure of nanosize $La_{0.7}Sr_{0.3}MnO_3$ [11,12].

The particle size effect on the electron transport of manganites have been also investigated [8,13–16]. A magnetoresistance above 10 % was obtained in a field of 1 kOe for all the particles sizes (from 20 to 110 nm) of $La_{0.67}Ca_{0.33}MnO_3$ [8]. Both the resistivity and high-field magnetoresistance of $La_{2/3}Sr_{1/3}MnO_3$ manganite having the grain diameters ranging from 10 μm to 20 nm increase substantially as the particle size decreases, while the maximum magnetoresistance exhibited by the nanosize powders near the Curie temperature is found to be not sensitive to the particle size [13,14]. Unlike the bulk manganites, in nanostructured manganites a low field magnetoresistance was observed. The ultrafine (18 nm) $La_{2/3}Ca_{1/3}MnO_3$ powder is insulating from 5 to 300 K and is superparamagnetic above the blocking temperature corresponding to the peak in the ZFC magnetization [15]. When the temperature is below blocking temperature, the magnetoresistance is shown to be associated with the spin-polarized tunneling between grains. In Ref. 16, a model for the nanoparticles based on the existence of a noncollinear, amorphous surface layer at the grains was supposed to explain both the higher resistivity and the reduction of saturation magnetization in the smaller particle samples. It should be noted that a clear understanding of the magnetic and transport properties caused by nanostructuration of manganite is still lacking.

In this paper, we report on the synthesis and characterization of nanopowder $(La_{0.7}Sr_{0.3})_{0.9}Mn_{1.1}O_3$ manganites as well as on the study of influence of the nanostructure on their magnetic and transport properties.

The manganese–lanthanum–strontium manganite $(La_{0.7}Sr_{0.3})_{0.9}Mn_{1.1}O_3$ with high phase transition temperature (about of 360 K) has been studied. Since the excess manganese increases MRE [17], this compound is perspective for application in the high sensitive sensor of magnetic field [18,19]. A large magnetic moment at room temperature allows to use the nanoparticles of this manganite coated with appropriate macromolecules for application in biomedical diagnostic [20].

The format of the paper is as a follows. In Introduction, the analysis of papers devoted to the influence of grain size down to nanometric dimentions on the magnetic and transport properties manganites is presented.

In the first section, the brief information on the main experimental details, namely, nanosize samples preparation, crystalline structure, dc magnetization, ^{55}Mn nuclear magnetic resonance and resistance measurements, are reported. The application of a broad spectrum of experimental methods has allowed to obtain complete information on the particle size effect on a physical properties as well as on peculiarities of behavior of nanopowder $(La_{0.7}Sr_{0.3})_{0.9}Mn_{1.1}O_3$ manganite studied.

The grain size effect on magnetic properties is presented in the second section. Based on the experimental results, the magnetic moment is shown to depend strongly on the average particles size, $\langle d \rangle$, while both the magnetic phase transition temperature and the paramagnetic Curie–Weiss temperature change insignificantly with varying $\langle d \rangle$. There is a tendency towards a decrease of both magnetic moment and magnetic entropy with decreasing $\langle d \rangle$.

In the third section, we have focused on the transport properties changes caused by varying $\langle d \rangle$, basing on the results of resistance (ρ) measurements both in and without magnetic field. Temperature dependences of resistance show that the resistivity becomes higher with reducing the particles size at any temperatures.

The summary suggests that the nanoparticles size plays an important role in the formation of magnetic and transport properties.

1. Sample and experimental

The methods of preparation of manganite nanoparticles are nontrivial. In this work, the co-precipitation technology of production of nanosize stochiometric manganese–lanthanum–strontium perovskites has been used. The mixture of

stoichiometric amounts of high purity Mn_3O_4, La_2O_3 and $SrCO_3$ powders was dissolved in diluted nitric acid. This solution was evaporated to dryness, and then, it was fired at 500 °C to decompose the nitrates. Dry remainder was thoroughly grinded and again was annealed at different (800, 900 and 950 °C) for duration of 20 h in air, followed by a slow cooling down to T_{room}. The resulting material was repeatedly grinded, and the nanopowders with the average particle size of 40, 75 and 100 nm were obtained (Table 1). The grain size of nanopowders obtained was estimated by the method of low-temperature adsorption of argon known as BET's method [21]. This method has allowed to determine the specific surface (S_{SS}) and then to calculate the average particles size $\langle d \rangle$ knowing the x-ray density (σ_γ). The average grains size was also determined by x-ray diffraction measurement (XRD) using Scherrer's relation $D = \lambda/B\cos\theta$, where D is the magnitude of grains size, θ is the Bragg angle, B is the difference between half-widths of the Bragg reflex of nanopowder and standard. The standard was Si powder with the size 10 μm. A good agreement between these methods was obtained (Table 1).

Table 1. Physical and chemical characteristics of nanopowders prepared at temperatures of 950 (PS1), 900 (PS2) and 800 (PS3) °C

Sample	Lattice parameters		Specific surface	Density	Particle size from S_{SS}	Particle size from XRD
	a, Å	α, deg	S_{SS}, m^2/g	σ_γ, g/cm^3	$\langle d \rangle$, nm	$\langle d \rangle$, nm
PS1	5.465	60.38	1.7 ± 0.3	5.891	100 ± 20	90 ± 17
PS2	5.467	60.37	2.3 ± 0.4	5.893	75 ± 10	70 ± 8
PS3	5.470	60.35	5.8 ± 0.7	5.895	40 ± 5	37 ± 5

The magnetization measurements were performed with a vibrating sample magnetometer in the temperature range of 5–375 K and in magnetic fields from 500 Oe to 10 kOe. Both zero-field-cooled (ZFC) and field-cooled (FC) magnetization vs. temperature and at selected magnetic field were measured.

^{55}Mn nuclear magnetic resonance (NMR) spectra were recorded using a two-pulse spin echo method at temperature between 77 and 300 K and zero external magnetic field. A noncoherent spectrometer with a frequency sweep and box-car detector signal averaging has used.

The resistance (ρ) and magnetoresistive effect, $\Delta\rho/\rho_0 = (\rho_0 - \rho_H)/\rho_0$, have been measured by four-probe method in a temperature range of 4.2–300 K and in magnetic field of $H = 4$ kOe. Contacts were made using silver paste.

For magnetic, transport and resonance measurements, the nanopowders obtained were pressed at room temperature under pressure of 0.2 GPa into pellets 1.5 mm thick and 6 mm in diameter.

In this paper, the experimental and theoretical studies of magnetism and transport in the $(La_{0.7}Sr_{0.3})_{0.9}Mn_{1.1}O_3$ manganites with the nanoparticle sizes of $\langle d \rangle = 100$ (PS1), 75 (PS2) and 40 (PS3) nm are presented.

The crystallographic structure and lattice parameters of the samples (Table 1) were determined with room temperature x-ray powder diffractometer using the Cu K_α radiation XRD patterns were recorded on a Philips PW-3710X'PERT diffractometer. The 2θ scan are performed with the steps of 0.01 and a counting time of 5 s step. The data are analyzed with the Rietveld-type refinement software FullProf program. The obtained results indicate that the samples are homogeneous single phase compounds and have rhombohedral structure (the space group $R\bar{3}c$). The atoms occupy the following positions: (La,Sr) in the 2*a* site 1/4,1/4,1/4; Mn in the 2*b* 0,0,0 and O in 6*e* $x,1/2-x,1/4$.

The change of particle size from 100 to 40 nm was established to produce an insignificant increase of the a lattice parameter and an insignificant deviation of the α edge from 60°.

2. Magnetic properties

2.1. dc magnetization

The temperature variation of dc magnetization for three nanopowders under consideration in magnetic field of 0.05 T near the phase transition is depicted in Fig. 1.

For all samples the ferromagnetic-like behavior is observed. Near the phase transition temperature, the magnetization begins to rise sharply with decreasing temperature indicating the onset of ferromagnetic ordering and tends to the saturation. It is seen that the magnetization is strongly influenced by the particles size and decreases as the grain size of the particles diminishes. In inset to Fig. 1 the $M_{FC}(T)$ dependences for the PS3 sample in magnetic

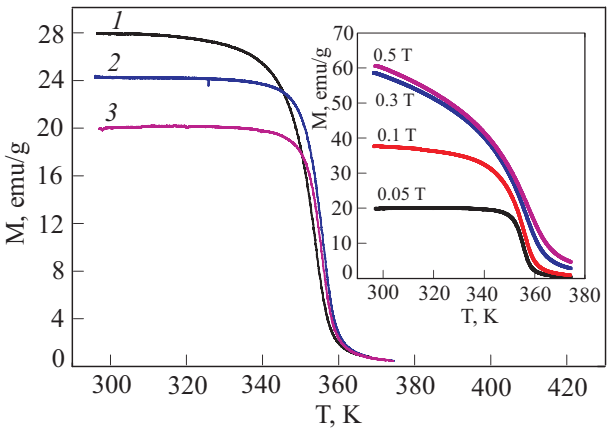

Fig. 1. (Color online) Temperature variation of magnetization for the PS1, PS2 and PS3 (curves *1–3*, respectively) nanopowders under consideration in magnetic field of 0.05 T. Inset: $M_{FC}(T)$ dependences for the PS3 sample in magnetic fields of 0.05–0.5 T.

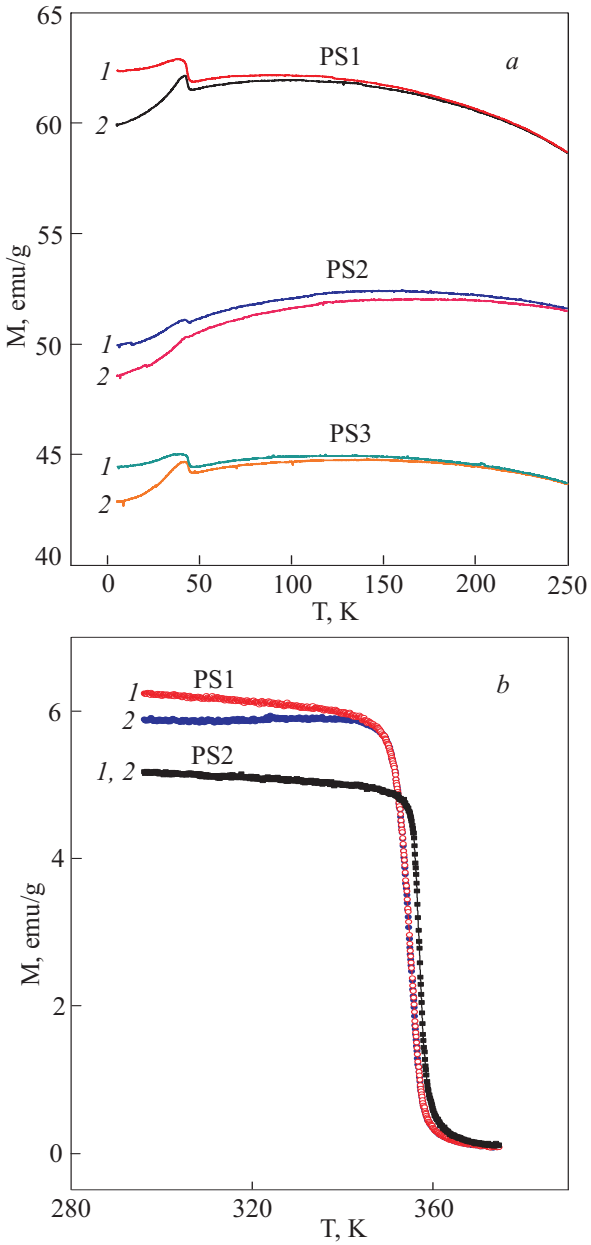

Fig. 2. (Color online) Low-temperature field-cooled (M_{FC}) (curve *1*) and zero-field-cooled (M_{ZFC}) (curve *2*) magnetization recorded in magnetic field of 0.1 T for PS1, PS2, PS3 samples (*a*). The FC and ZFC magnetization (curves *1* and *2*, respectively) as a function of temperature for PS1 and PS2 in field of 100 Oe (*b*).

fields of 0.05–0.5 T are shown. The influence of magnetic field on the $M_{FC}(T)$ dependences for the another samples is similar.

The low-temperature field-cooled (M_{FC}) and zero-field-cooled (M_{ZFC}) magnetization recorded in magnetic field of 0.1 T for all samples are presented in Fig. 2,*a*.

Figure 2,*b* shows the FC and ZFC magnetization for PS1 and PS2 as a function of temperature near phase transition. The insignificant difference between FC and ZFC magnetization, which begins to diverge below 340, 300 and 275 K for PS1, PS2 and PS3, respectively, and increases with decreasing temperature, indicates the presence of a small magnetic anisotropy. The difference between M_{ZFC} and M_{FC} magnetization diminishes in magnetic field and disappears between 1 and 3 kOe. The local maximum observed in the magnetization curves at low temperatures (about 42 K) suggests a possible frustration effect induced by a competition from different magnetic interactions, that can result in spin canting at lower temperature due to an excess manganese [17]. This fact could be consist with an antiferromagnetic ordering in Mn^{3+}–O– Mn^{4+} clusters [22].

The analysis of high-temperature dc susceptibilities (M/H) of samples studied was performed using the Curve–Weiss (CW) law:

$$\chi(T) = \chi_0 + \frac{C}{T - \theta}, \qquad (1)$$

where χ_0 is the background susceptibility, the Curie constant $C = \mu_{\text{eff}}^2/3k_B$, $\mu_{\text{eff}}(S) = \mu_B g\sqrt{S(S+1)}$ is the effective magnetic moment, θ is the paramagnetic CW temperature.

The experimental $H/M(T)$ dependences for samples PS2 in fields of H = 0.05, 0.1, 0.3 and 0.5 T are presented in Fig. 3.

Similar $H/M(T)$ dependences were obtained for the another samples. The fitting of the experimental $M(T)$ dependences to the CW law (1) has shown that $H/M(T)$ curves as a function of temperature are linear at temperatures above T_C and obey the CW law for all samples. A root-mean square error of fitting is equal to ≈ 0.2 %. The CW temperatures, θ, calculated as a result of a fitting of CW law to the experimental data were found to have the positive sign that is indicative of dominant ferromagnetic interactions. The θ temperatures do not depend practically on changes of $\langle d \rangle$. Using the CW constant values the effective numbers of Bohr magneton, n_{eff}, were calculated. The χ_0, C, θ, T_C, n_{eff} values of as a function of $\langle d \rangle$ are summarized in Table 2. In magnetic fields from 0.1 to

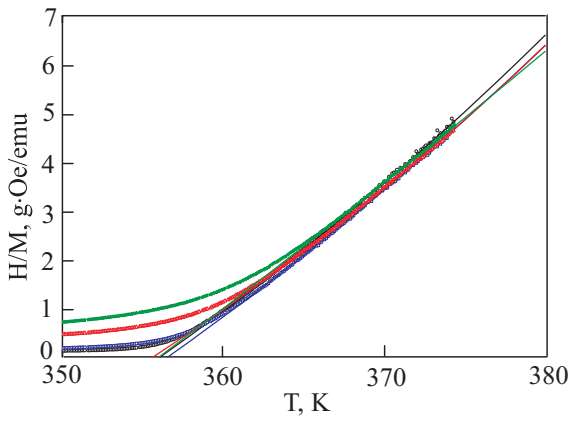

Fig. 3. (Color online) Experimental $H/M(T)$ dependences for PS2 sample in fields of H = 0.05, 0.1, 0.3 and 0.5 T. (Fitting of the experimental $M(T)$ dependences to the CW law is shown by solid lines.)

0.5 T, the χ_0, C and n_{eff} parameters calculated decrease insignificantly.

Table 2. The parameters obtained from fitting to the Curie–Weiss law

Sample	Parameter				
	χ_0, emu/mol	C, emu · K/mol	θ, K	n_{eff}	T_C, K
			$H = 0.05$ T		
PS1	–0.0233	4.98	354	6.3	354
PS2	–0.0276	4.28	356	5.9	356
PS3	–0.016	3.62	355	5.4	354
			$H = 0.3$ T		
PS1	–0.0099	4.29	354	5.86	355
PS2	–0.0333	4.62	357	6.08	357
PS3	–0.0215	3.87	355	5.57	355
			$H = 0.5$ T		
PS1	–0.0185	4.43	354	5.95	356
PS2	–0.0086	4.03	356	5.68	358
PS3	–	–	–	–	–

The theoretical estimation of the effective magnetic moment in nano-size manganites is of interest. In systems with variable valency of ions Mn^{3+} (concentration x) and Mn^{4+} (concentration $1-x$), the total magnetic moment (μ_{tot}) can be written in the form:

$$\mu_{tot}^2 = x\mu_{eff}^2(S_1) + (1-x)\mu_{eff}^2(S_2), \qquad (2)$$

where $S_1 = 2$ and $S_2 = 3/2$ are the spins of Mn^{3+} and Mn^{4+} ions, respectively, $x = 0.7$ is the Mn^{3+} concentration and g factor is equal to 2. The high value of the total moment equal to $\mu_{tot} = 4.62\ \mu_B$ was obtained. The μ_{tot} value is between the spin-only values for Mn^{3+} ($4.9\ \mu_B$) and Mn^{4+} ($3.87\ \mu_B$) ions. In our case, the effective number of Bohr magnetons determined experimentally are higher than the total effective moment value calculated. Similar situation was observed in Ref. 23, where for the system $La_{0.93}MnO_3$ with Mn^{4+} concentration $1-x = 0.21$ the experimental and calculated values of the total effective moment are equal to 4.7 and 5.8 μ_B, respectively. It was concluded that in a paramagnetic phase the polaron effects are responsible for formation of the magnetic clusters. As the result, it leads to increase of Curie constants and, respectively, to increase of the total effective magnetic moment.

The FM phase transition temperatures (T_C) were defined from peak of dM/dT in the $M(T)$ dependence. Despite the particle size difference, the Curie temperatures were found to coincide practically (± 2 K) for all samples studied (Table 2). This means that the inner parts (cores) of grains in all nanopowders are magnetically identical, i.e., a Mn^{3+}/Mn^{4+} ratio in the nanoparticles is similar, and their contribution to the magnetization is nearly the same. It agrees with a model of the nanoparticles presented in Ref. 16. The T_C temperatures determined are close to those in a bulk manganite of the same composition.

Additional information on the magnetic properties was obtained by the measurements of both the $M(T)$ magnetization in applied magnetic field and $M(H)$ isotherms. The magnetization is highly dependent on the applied magnetic field (inset to Fig. 1). The paramagnet–ferromagnet phase transition in magnetic field becomes broader and the $M(T)$ dependence shifts towards high temperatures what indicates a extension of the FM phase. Figure 4 shows a comparison of field dependences of magnetization, $M(H)$, dependences for all samples at 5 and 300 K. The magnetization isotherms display a ferromagnetic behavior and reach the saturation at low temperatures above 0.4 T. The magnetization decreases with reducing $\langle d \rangle$. The magnetic moment values observed in nanoparticles studied are close to the reported values [8,9]. The field dependences of magnetization at 1 T and 5 K correspond to uniform ferromagnet having the magnetic moments of 3.4, 3.2 and 3.1 μ_B/Mn for the PS1, PS2 and PS3 samples, respectively, which are noticeably smaller than the value of moment equal to 3.7 μ_B/Mn taking into account the presence of about 30 % Mn^{4+} ions in the samples studied. It can be supposed to be attributed to the presence of noncollinear interface layers between grains for the smaller size particles.

Figure 4 shows that at $T < T_C$ in small fields we have usual magnetic reversal of domains with a susceptibility $1/4\pi N$, where N is the demagnetizing factor of the sample. In fields of $H > 0.2$ T, the basic contribution to increasing magnetization is connected with reorientation of local spin along magnetic field. In this field range, the

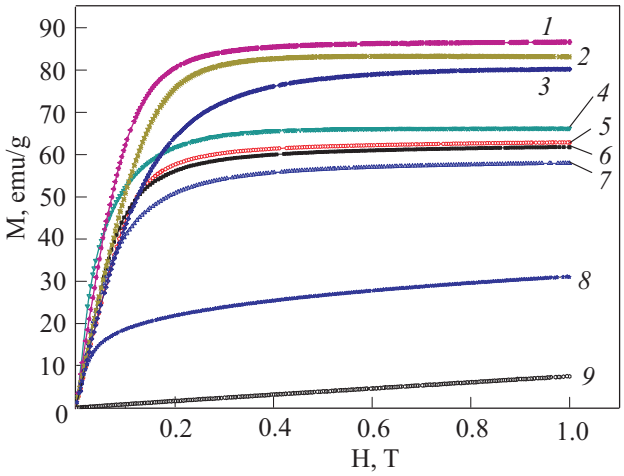

Fig. 4. (Color online) Comparison of $M(H)$ dependences at 5 K for PS1, PS2 and PS3 (curves *1–3*, respectively), at $T = 300$ K for ceramic, PS1, PS2 and PS3 (curves *4*, *5*, *6* and *7*, respectively) and at 351 and 373 K for PS1 (curves *8*, *9*, respectively).

thermodynamic behavior typical for electronic spin system with the double exchange is realized.

The measurements of hysteresis loops in field ±1 T show that a coercive field (H_{coerc}) is small for all nanopowders. A coercivity at $T = 4.2$ K increases from 10 to 25 Oe with decreasing $\langle d \rangle$ from 100 to 40 nm (Fig. 5). A small value of coercive field indicates a very weak anisotropy energy and testifies on soft ferromagnetic behavior of the samples studied. As known, a multidomain particles have such low coercive fields. The remanent magnetization (M_{rem}) also changes slightly with changing $\langle d \rangle$.

To exclude the influence of magnetic dipole interactions in weak fields (demagnetizing field), the Arrot's method [24] was used to describe the temperature behavior of spontaneous magnetization in strong fields near T_C.

In Fig. 6, the experimental Arrot's curves for sample PS3 near the phase transition are presented. Similar curves were obtained for PS1 and PS2. The temperature dependence of spontaneous magnetization was determined by linear fitting of the experimental data to Arrot's curves:

$$M^2(H,T) = A + B\frac{H}{M(H,T)}, \qquad (3)$$

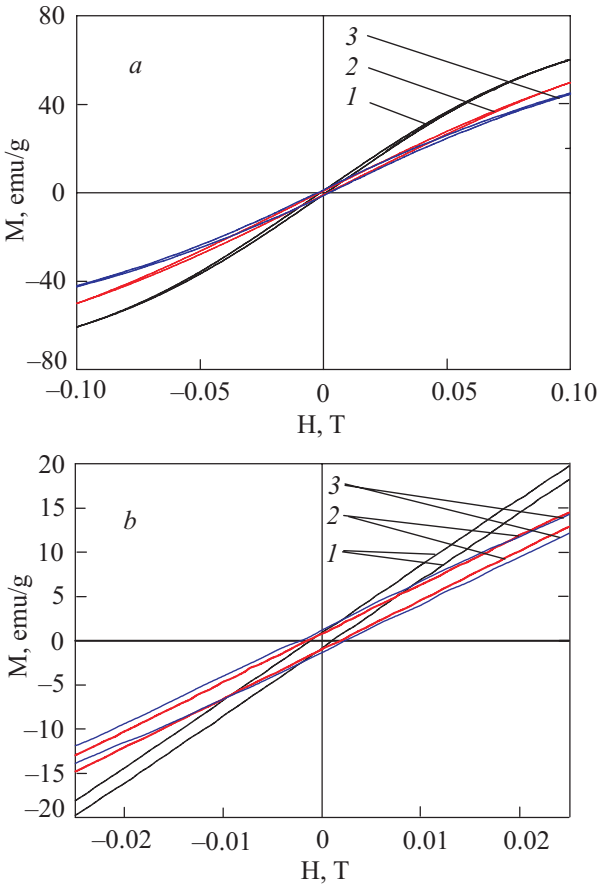

Fig. 5. (Color online) $M(H)$ dependences (*a*) and the hysteresis loops (*b*) for the PS1, PS2 and PS3 (the curves *1*, *2* and *3*, respectively) at $T = 4.2$ K.

where A and B are the fitting parameters. Knowing the A factor, it is possible to find spontaneous magnetization, $M_0(T)$, as $M_0(T) = \sqrt{A}$, as well as the field dependence of spontaneous magnetization, $M_0(H)$, without taking into account of influence of domain structure.

The saturation magnetization $M_0(T)$ at temperatures below 200 K was determined by fitting to dependence [25]

$$M(H,T) = M_0(T) - \frac{a_1}{H} - \frac{a_2}{H^2}, \qquad (4)$$

where a_1 and a_2 are the fitting constants.

The left inset to Fig. 6 shows the experimental field dependences of magnetization (points) and corresponding interpolation curves $M(H)$ (lines). Both Fig. 4 and the right inset to Fig. 6, where the temperature variation of the spontaneous magnetic moment for the samples with various grain sizes is depicted, confirm that the magnetic moment decreases with decreasing particles size. It may be due to the surface effect, since in FM and AFM oxides with the particle size less than 100 nm the local order of atoms situated in the surface layer can differ considerably from that of the interior atoms [9,14,16]. An outer shell of particles will contain most of the oxygen vacancies and faults in the crystallographic structure that leads to magnetically disordered state. The atom disorder affecting the magnetic interactions can lead to a canting of the surface spins, or to the state when the outer layer has no net moment.

The comparison of the experimental and calculated dependences of spontaneous magnetization for nanoparticles is of interest. To perform such comparison it is necessary to know two basic parameters in the theory of double exchange: the e_g electron bandwidth, W, and the

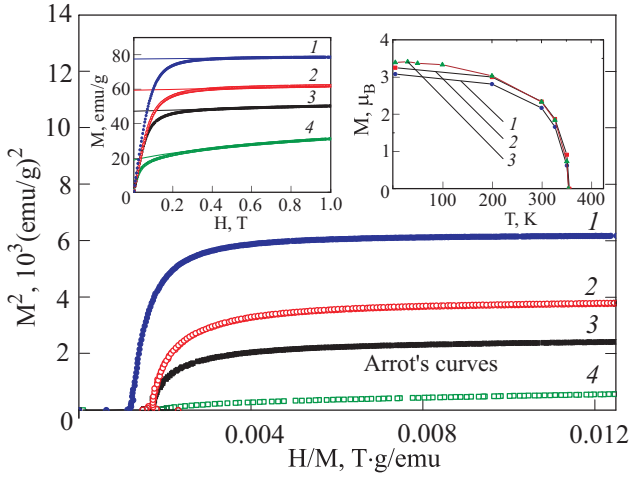

Fig. 6. (Color online) Experimental Arrot's curves for samples PS3 at temperatures of 200, 300, 327 and 351 K (curves *1–4*, respectively). Left inset: experimental field dependences of magnetization (points) and corresponding interpolation curves $M(H)$ (lines). Right inset: the variation of the spontaneous magnetic moment with grain sizes for PS3, PS2 and PS1 samples (curve *1*, *2* and *3*, respectively).

site concentration of e_g electrons, n. According to the chemical formula, the Mn^{3+} concentration is equal to 0.7. If all the e_g electrons participate in a double exchange, it may be suggested that $n = 0.7$. In the frame of double exchange model [26,27], the concentration dependence of the Curie temperature (in a unit of bandwidth, T_C/W) has been calculated in Ref. 28. In particular, $T_C/W = 0.0211$ at $n = 0.7$ and $W = 1.45$ eV for the $T_C = 355$ K.

In Ref. 27, the self-consistent equations for an average site spin of $\langle\sigma^z + S_0^z\rangle$, including spin of e_g electron (σ), spin of Mn^{4+} ion (S_0^z) and chemical potential (μ), are presented in the form

$$\frac{1}{8}(5-n)+\frac{1}{4}\langle\sigma^z + S_0^z\rangle = \langle F^{+0}\rangle_1 - \nu_\downarrow \langle F^{-0}\rangle ,$$
$$\frac{1}{8}(5-n)+\frac{1}{4}\langle\sigma^z + S_0^z\rangle = \langle F^{-0}\rangle_1 - \nu_\uparrow \langle F^{+0}\rangle , \quad (5)$$

where $\langle F^{+0}\rangle$ and $\langle F^{-0}\rangle$ are the average probability of electron–hole state, the chemical potential is included in $\langle F^{\sigma 0}\rangle_1$ and

$$\nu_i \langle F^{i0}\rangle = \frac{1}{4N}\sum_{\mathbf{q}} (f(E_{\mathbf{q}i}) - f(-\varepsilon_{0i})) . \quad (6)$$

Here $f(x)$ is the Fermi function, $E_{\mathbf{q}i} = -\varepsilon_{0i} + t(\mathbf{q})\langle F^{i0}\rangle$, ε_{0i} are the mean field energy levels of Mn ions and $t(\mathbf{q})$ the Fourier representation of the hopping integral. The difference of the mean field energy of hole and electron with spin upwards or downwards is of

$$\varepsilon_{0i} = \mu + i\frac{\mu_B g\tilde{H}}{2}, \text{ where } \tilde{H} = H + \frac{J(0)}{\mu_B g}\langle\sigma^z + S_0^z\rangle ,$$

$J(0)$ is the indirect exchange parameter and $i = +1$ or -1 for the projection of spin electron upwards and downwards, respectively. The average probability of electron–hole state with spin upwards or downwards is defined by the expression

$$\langle F^{i0}\rangle = \frac{1}{8}(5-n)+\frac{i}{4}\langle\sigma^z + S_0^z\rangle , \quad (7)$$

where the sign $\langle\ldots\rangle$ designates averaging over the full Hamiltonian. The average expression of F^{i0} operator in a molecular field approximation has the simple form:

$$\langle F^{i0}\rangle_0 = n\langle S_2^z\rangle_0 + (1-n)\langle S_{3/2}^z\rangle_0 . \quad (8)$$

S_2^z and $S_{3/2}^z$ spin operators designate the z projections of $S = 2$ and $S = 3/2$ spins, respectively. The $\langle F^{i0}\rangle_1$ value in the expression (5) has the same form, but in which the mean field ε_{01} and ε_{0-1} levels are shifted on energies of electronic density fluctuations, $\delta\mu_\downarrow/4$ and $\delta\mu_\uparrow/4$, respectively, where

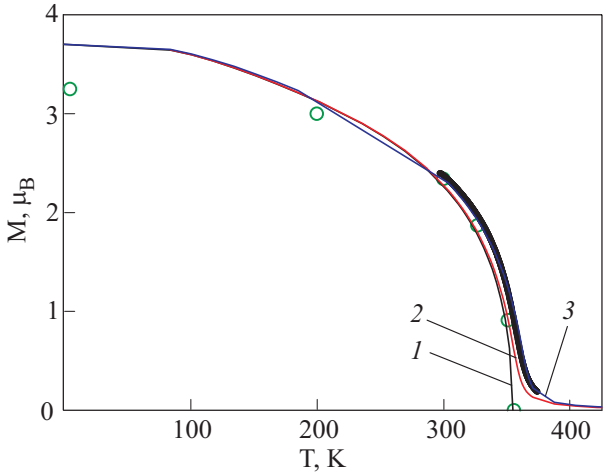

Fig. 7. (Color online) Magnetic moment as a function of temperature calculated for $n = 0.7$ at $H = 0$ and $J(0) = 0$ (curve *1*) and in field of $H = 0.5$ T at $H/W = 3.98\cdot10^{-5}$ (curve *2*) and at $J(0)/W = 1.19\cdot10^{-4}$ (curve *3*). Experimental temperature dependences of the spontaneous magnetic moment for the sample PS2 near the phase transition at $H = 0$ (open circles) and in field of $H = 0.5$ T (full circles).

$$\delta\mu_i = \frac{1}{N}\sum_{\mathbf{q}} t(\mathbf{q}) f(E_{\mathbf{q}i}) . \quad (9)$$

The set of Eqs. (5) was solved numerically for $n = 0.7$ in field of $H = 0$ at $J(0) = 0$ and in field of $H = 0.5$ T at $J(0) = 0$ and $J(0) = 2$ K, that corresponds to the relations of $H/W = 3.98\cdot10^{-5}$ and $J(0)/W = 1.19\cdot10^{-4}$. The calculation results of the magnetic moment presented in Fig. 7 show the influence of magnetic field on the phase transition and an additional biasing of phase transition due to an indirect exchange.

Comparison of experimental and calculated temperature dependences of the spontaneous magnetic moment for the PS2 sample near the phase transition (Fig. 7) shows that the spontaneous magnetization both in magnetic field and without field is well described in the frame of the double exchange model.

2.2. Nuclear magnetic resonance spectra

The ^{55}Mn nuclear magnetic resonance (NMR) spectra were obtained by measuring the integrated intensity of the spin-echo versus frequency. In Fig. 8,*a*,*b* the NMR spectra for PS1 and PS3 are illustrated. The spectrum for the PS2 sample is the same as for PS3 (it is not given). The ^{55}Mn NMR studies have been performed at 77 K when the localized Mn^{3+} and Mn^{4+} states are frequency not resolved. The NMR signal detected at $f_{res} \approx 375$ MHz is typical of mixed valence metallic-like ferromagnetic manganites and corresponds to fast hopping of electron–holes among Mn sites [12]. The NMR spectra lines for PS2 and PS3 (Fig. 8,*b*) are practically symmetrical about f_{res} indicating the homogeneity of nanoparticles intrinsic ferromagnetic region.

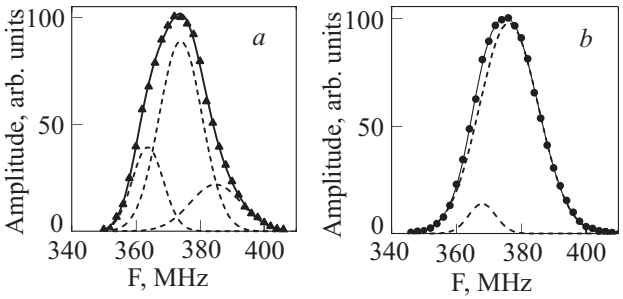

Fig. 8. ^{55}Mn nuclear magnetic resonance spectra for PS1 (*a*) and PS3 (*b*) at 77 K.

Unlike the PS3 and PS2 samples, the NMR spectrum for PS1 is broadened (Fig. 8,*a*). Asymmetrical NMR spectrum for PS1 is due to nonhomogeneity of manganese ions environment by both La^{3+} and Sr^{2+} ions and defects. It is necessary to note the closeness of spin–spin relaxation time ($\tau_2 \approx 10$ μs) for all systems. Computer decomposition of NMR spectrum has shown that it resolves on three components with maximum frequencies of 363.7, 374.0 and 384.9 MHz for PS1 and on two components with maximum frequencies of 361.0 and 376.2 MHz for two other nanopowders, that is indicative of nonequivalence of magnetic state of manganese ions in samples with various particle sizes. In the case of PS1, it is caused by larger deficiency of perovskite structures involving the anion and cation vacancies as well as nanostructural clusters. In the case of PS2 and PS3, it is due to smaller concentration of vacancies. The increase of basic component of resonant frequency ($\Delta F = 376.2 - 374.0 = 2.2$ MHz) also indicates smaller deficiency perovskite structures for PS3 and PS2 nanopowders. Note that in NMR spectra a component with frequency $F = 387$ MHz is close to frequency of localized Mn^{3+} states, and a component with frequency $F =$ = 368 MHz is close to frequency of Mn^{4+} states.

2.3. Magnetocaloric effect

In this paper, the magnetocaloric effect (MCE) characterazing the magnetic entropy (ΔS_M) change produced by changes of the magnetic field applied to the system was calculated from initial magnetization curves.

Using the Arrot curves (see the lines in Fig. 6) the $M(H)$ dependences and spontaneous magnetization M_0 at $H = 0$ were obtained. For above temperatures we have used the spline interpolation to find the $M(H,T)$ dependence. The temperature dependence of ΔS_M was calculated using the relation [25]

$$\Delta S_M(T,H) = \int_0^H \left(\frac{\partial M(T,H')}{\partial T} \right)_{H'} dH'. \qquad (10)$$

Knowing the $M(H,T)$ dependence, we have found the derivative $\partial M(T,H')/\partial T$, and substituting it in Eq. (10) $\Delta S_M(T,H)$ was calculated.

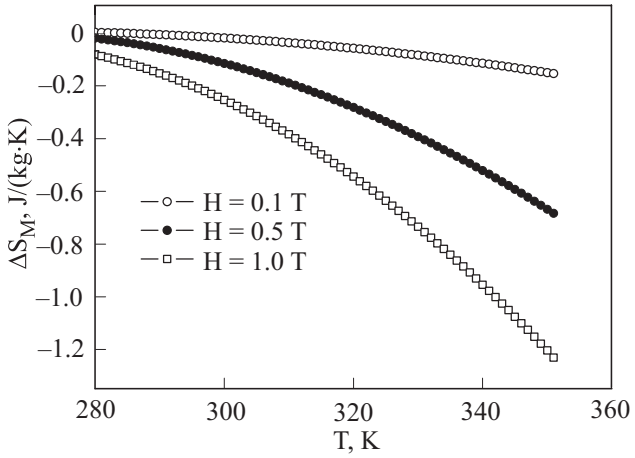

Fig. 9. Temperature dependences of ΔS_M at various magnetic fields for the PS3 sample.

In Fig. 9, a change of the absolute ΔS_M value in the magnetoordered phase as a function of temperature at different magnetic fields for the PS3 sample ($d = 40$ nm) is shown. Similar $\Delta S_M(T)$ dependences were obtained for other nanosize samples. The $\Delta S_M(T)$ dependences in the paramagnetic phase (above T_C) were not calculated, because the $M(H)$ were not measured. Therefore, a $\Delta S_M(T)$ peak around the magnetic phase transition was not observed. As it is seen in Fig. 9, the absolute value of magnetic entropy increases with increasing applied magnetic field. The absolute $\Delta S_M(T)$ value was found to decrease for the small particles. This behavior can be explained with the model of the nanoparticles composed of both an inner core with physical properties similar to the bulk and an outer shell. An outer shell has disordered magnetic structure. Its role increases with reducing particle size as $1/D$ [15], where D is the particle size. According to the relation (10) the magnetic entropy $\Delta S_M(T)$ is depended on the magnetization value. Therefore, the decrease of absolute values of $\Delta S_M(T)$ can be explained by decreasing magnetic moment of nanopowders caused by the surface effect as the grain size decreases. The relative surface contribution, or the surface/volume of the grains ratio, increases due to the larger surface area of the small particles. Thus, the total magnetocaloric effect reduces as the particle size diminishes, since the contribution of the outer shell having the disordered magnetic state to MCE will increase.

3. Transport properties

The magnetic properties was shown to be markedly affected by the grain size. Since the magnetic properties of manganites are closely connected to their transport properties, it is of interest to study the particles size effect on the resistivity and magnetoresistance. The temperature dependences of resistance, $\rho(T)$, presented in Fig. 10,

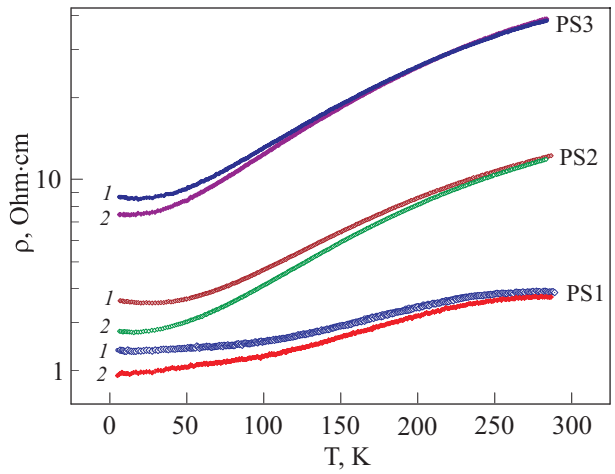

Fig. 10. (Color online) Temperature dependence of resistance, $\rho(T)$, for PS3, PS2 and PS1 samples at $H = 0$ (curve *1*) and $H = 4$ kOe (curve *2*), respectively.

show that the resistivity becomes higher with reducing the particles size at any temperatures.

The higher resistivity observed in the smaller particles can be caused by the potential barrier between the nanoparticles as a result of the presence of an amorphous (or disordered) interface layers between grains in outermost shell [9,10,16]. The one of factor affecting the electron mobility is the larger surface area associated with the small grain size. The energy level of the Mn ions at the surface is different from that inside the grain. Thus, e_g electrons near the surface are likely to be localized and the interfaces between grains are insulating [15]. An insulating-like behavior becomes apparent below ≈ 70 K in the $\rho(T)$ dependence for the sample having the smallest grain size.

The magnetoresistance (MR) for all the nanoparticles studied is of order of 13–18 % at low temperatures in magnetic field of $H = 4$ kOe, that agrees with the MR value for La–Sr–Mn system [29]. This observation implies that a substantial part of MR at low temperatures arises from the grain boundaries.

Conclusions

In this paper magnetic, transport, thermal and resonance measurements of nanoparticle $(La_{0.7}Sr_{0.3})_{0.9}Mn_{1.1}O_3$ manganite having an averaged grain size ranging from 40 to 100 nm have been carried out. The experimental data have shown that the nanostructuration of the grains plays an important role in the magnetism and transport of manganite studied. Its properties are strongly depended on the surface effects related to the grain sizes. The magnetization of nanopowders decreases with decreasing particle size unlike that the phase transition temperature does not show significant difference in respect to bulk counterpart. The simplest explanation of magnetic moment decrease is the existence of a noncollinear spin structure, or magnetically «dead» layer at the surface of nanoparticles as a result of the atom disorder in the surface layer. The relative surface contribution, or the surface/volume of the grains ratio, increases due to the larger surface area of the small particles, and therefore their spontaneous magnetization is diminished. This explanation agrees with a model of the nanoparticles composed of an inner core with physical properties similar to the bulk and an outer shell with oxygen vacancies, defects and etc. [16]. However, the spin disorder mechanism at the nanoparticle surface needs to be ascertained. The magnetic entropy $\Delta S_M(T)$ was shown to increase with increasing applied magnetic field and its absolute value is smaller for the small particles. The total magnetocaloric effect reduces as the particle size diminishes, since the contribution of the outer shell having the disordered magnetic state to MCE will increase. The a presence of an amorphous (or disordered) interface layers between grains also affects the transport properties. The resistivity becomes higher with reducing the particles size due to increasing surface contribution. The MR value of the nanoparticle samples increases to 13–18 % with reducing particle size in field of 4 kOe at 4.2 K. This observation shows that a substantial part of the MR at low temperatures arises from the grain boundaries.

Acknowledgments

This work was in part of the research program of the Polish National Scientific Network «Materials with strongly correlated electrons».

1. S.T. Jin, T.H. Tielfel, M. McCormack, R.A. Fastnacht, R. Ramesh, and L.H. Chen, *Scienc*e **264**, 413 (1994).
2. A.P. Ramirez, *J. Phys.: Condens. Matter* **9**, 8171 (1997).
3. J.M.D. Coey, M. Viret, and S. von Molnar, *Adv. Phys*. **48**, 167 (1999).
4. V. Spasojevic, D. Markovic, V. Kusigerski, B. Antic, S. Boskovic, M. Mitric, M. Vlajic, V. Krstic, and B. Matovic, *J. Alloys & Comp*. **442**, 197 (2007).
5. C. Acha, G. Garbarino, and A.G. Leyva, *Physica B: Condens. Matter* **398**, 212 (2007).
6. V. Markovich, I. Fita, D. Mogilyansky, A. Wisniewski, R. Puzniak, L. Titelman, L. Vradman, M. Herskowitz, and G. Gorodetsky, *J. Phys.: Condens. Matter* **19**, 346210 (2007).
7. R. Rajagopal, J. Mona, S.N. Kale, T. Bala, R. Pasricha, P. Poddar, M. Sastry, L.V. Prasad, D.C. Kundaliya, and S.B. Ogale, *Appl. Phys. Lett*. **89**, 023107 (2006).
8. Y.W. Duan, X.L. Kou, and J.G. Li, *Physica B: Condens. Matter* **355**, 250 (2005).
9. R.D. Sanchez, J. Rivas, C. Vazquez-Vazquez, A. Lopez-Quintela, M.T. Causa, M. Tovar, and S. Oseroff, *Appl. Phys. Lett*. **68**, 134 (1996).
10. S. Roy, I. Dubenko, D.D. Edorh, and N. Ali, *J. Appl. Phys*. **96**, 1202 (2004).
11. V.N. Krivoruchko, T. Konstantinova, A. Mazur, A. Prokhorov, and V. Varyukhin, *J. Magn. Magn. Mater*. **300**, e122 (2006).

12. M. Bibes, L.I. Balcells, J. Fontcuberta, M. Vojcik, S. Nadolski, and E. Jedryka, *Appl. Phys. Lett*. **82**, 928 (2003).
13. R. Mahesh, R. Mahendiran, A.K. Raychaudhuri, and C.N.R. Rao, *Appl. Phys. Lett*. **68**, 2291 (1996).
14. L.I. Balcells, J. Fontcuberta, B. Martinez, and X. Obradors, *Phys. Rev*. **B58**, R14697 (1998).
15. R.-W. Li, H. Xiong, J.-R. Sun, Q.-A. Li, Z.-H. Wang, J. Zhang, and B.-G. Shen, *J. Phys*.: *Condens. Matter* **13**, 141 (2001).
16. M.A. Lopez-Quintela, L.E. Hueso, J. Rivas, and F. Rivadulla, *Nanotechnology* **14**, 212 (2003).
17. V. Dyakonov, I. Fita, E. Zubov, V. Pashchenko, V. Mikhaylov, V. Prokopenko, Yu. Bukhantsev, M. Atciszewska, W. Dobrowolski, A. Nabialek, and H. Szymczak, *J. Magn. Magn. Mater.* **246**, 40 (2002).
18. L.I. Balcells, R. Enrich, J. Mora, A. Calleja, J. Fontcuberta, and X. Obradors, *Appl. Phys. Lett*. **69**, 1486 (1996).
19. V.P. Pashchenko, M.I. Nosanov, and A.A. Shemjakov, *High Sensitive Sensor with Magnetoresistive Film*, Patent UA 69798 A (Bulletin 9, 2004).
20. Q.A. Pankhurst, J. Connolly, S.K. Jones, and L. Dobson, *J. Phys*. **D36**, R167 (2000).
21. S. Brunauer, P.H. Emmett, and E. Teller, *J. Am*. *Chem. Soc*. **60**, 309 (1938).
22. B. Raveau, Y.M. Zhao, C. Martin, M. Hervieu, and A. Maignan, *J. Solid State Chem*. **149**, 203 (2000).
23. S. de Brion, F. Ciorcas, G. Chouteau, P. Lejay, P. Radaelli, and C. Chaillout, *Phys. Rev*. **B59**, 1304 (1999).
24. A. Arrot, *Phys. Rev.* **108**, 1394 (1957).
25. S.V. Vonsovskii, *Magnetism*, Nauka, Moscow (1971), p. 1032 [Translated into English (New York: J. Wiley, 1974)].
26. C. Zener, *Phys. Rev*. **82**, 403 (1951).
27. P.-G. de Gennes, *Phys. Re*v. **B118**, 141 (1960).
28. E.E. Zubov, V.P. Dyakonov, and H. Szymczak, *J. Phys.: Condens. Matter* **18**, 6699 (2006).
29. S. Zhou and J.B. Goodenough, *Phys. Rev*. **B68**, 054403 (2003).